Electronic Supplementary Material (ESI) for ChemComm.

Supporting Information

Non-Precious Bimetallic Catalysts for Selective Dehydrogenation of an Organic Chemical Hydride System

Anaam H. Al-ShaikhAli, Abdesslem Jedidi, Luigi Cavallo, and Kazuhiro Takanabe

Division of Physical Sciences and Engineering, KAUST Catalysis Center (KCC),

King Abdullah University of Science and Technology (KAUST)

4700 KAUST, Thuwal 23955-6900, Saudi Arabia.

kazuhiro.takanabe@kaust.edu.sa

http://kcc.kaust.edu.sa

http://catec.kaust.edu.sa; http://kc2l.kaust.edu.sa

Experimental section

For the synthesis of mono-metallic catalysts (Ni, Zn, Sn, Ag, and In) supported on Al_2O_3 catalysts were synthesized using a homogenous deposition precipitation method. All the chemicals used were purchased from Sigma-Aldrich unless otherwise noted. For the synthesis, 4.73 g of urea (purity 99.5%) (i.e., molar ratio of urea/M = 100) was dissolved in 100 mL of Milli-Q water, and 0.025 M aqueous solution of the metal precursor (($NiCl_2 \cdot 6H_2O$ (purity 99.999%), $ZnNO_3 \cdot 6H_2O$ (purity ≥99%), $SnCl_4.5H_2O$ (purity 98%), $AgNO_3$ (purity 99.8-100.5%), and $InCl_3$ (purity 99.999%)), which corresponded to a metal content of 10 wt%, was added. For the support, Al_2O_3 (Alfa Aesar, 255 m^2/g, median pore 70 micron, total pore volume 1.14 cc/g, packing density 0.395 kg/L) was ground followed by heat treatment in static air at 500 °C. Next, 0.90 g of such obtained Al_2O_3 (218 $m^2\ g^{-1}$ by BET analysis) was added to the solution containing metal ions. The mixture was maintained in a three-neck spherical glass flask (500 mL) under an Ar atmosphere throughout the synthesis process to remove oxygen and organic byproducts, with vigorously stirring during the entire process. The pH was measured and determined to be 4 at this stage. After 1 h of stirring, the mixture was heated to 90 °C, which was maintained for 1 h to achieve urea hydrolysis under refluxing conditions. The mixture was cooled to room temperature. This step was followed by the addition of 100 mL of ethylene glycol (EG, purity ≥99%). After stirring overnight at room temperature, the solution was heated to 120 °C and maintained for 1 h under refluxing conditions. The obtained slurry was filtered and washed with copious amounts of water (600 mL) followed by 100 mL of ethanol (purity 99.96%, VWR chemical). The resulting sample was dried at 70 °C overnight. For the Ni-M bimetallic catalysts supported on Al_2O_3, a 0.025 M aqueous solution of the metal precursors corresponding to a total metal content of 8 wt% Ni and 2 wt% M were prepared for synthesis (M: Zn, Sn, Ag, and In). In addition, the catalysts were prepared by varying the ratio of Ni to Zn in weight percentage (i.e., Ni:Zn = 10:0, 9:1, 6:4, and 0:10).

The catalytic performance of the various transition metal mono- and bi-metallic based catalysts for the dehydrogenation of MCH was conducted in a flow type mode reactor under atmospheric pressure. In general, in each experiment, 20 mg of the catalyst were pelletized to 150-250 mesh and packed with a small amount of quartz wool in a U-shape tubular quartz reactor, which was vertically mounted inside the furnace. Prior to the test, the catalysts were reduced in situ for 30 min at 400 °C under a flow of H_2 (99.99999%, hydrogen generator NMH_2 300 DBS

analytical instrument, 30 mL min^{-1}) and Ar (purity 99.9999%, 30 mL min^{-1}). The catalytic reaction was carried out at 300 or 350 °C in the presence of both H_2 and Ar. The MCH feed was diluted with Ar, which was vaporized in a saturator at a temperature of 20 °C prior to feeding into the reactor. The resulting stream was fed into the catalytic reforming reactor. The products were detected by an online gas chromatograph (GC-8A Shimadzu) with Chromosorb W AW-DMCS equipped with a flame ionization detector (FID).

The powder X-ray diffraction (XRD) patterns were measured using a Bruker D8 Advanced A25 diffractometer equipped with a Cu-K_α (λ = 0.15418 nm) energy source at 40 kV and 40 mA. The inductively coupled plasma-optical emission spectrometry (ICP-OES) measurements were performed using an ICP-OES 720 series Agilent Technologies. The digestion of the material was performed in a microwave digestion oven (model ETHOS 1 from Milestone). The size of the metal nanoparticles of the synthesized catalysts was determined by bright-field transmission electron microscopy (TEM) on a FEI Titan ST electron microscope (Cs=1.2 mm; Cc=1.5 mm; 300 kV). Aberration-corrected high-angle annular dark-field scanning transmission electron microscopy (HAADF-STEM) was performed on a Titan G2 60–300 CT electron microscope at an accelerating voltage of 300 kV. The electron gun was used in the unfiltered mode, and the probe size during STEM analysis was estimated to be approximately 0.5 nm with a beam current of 0.08 nA. CO pulse chemisorption was carried out on an Autochem 2950 (Micromeritics, USA). The samples were purged with He (99.9999%, AHG, 40 mL min^{-1}) for 30 min, and then, H_2 (99.9999% AHG, 40 mL min^{-1}) was introduced into the instrument to reduce the Ni catalysts at 400 °C (10 °C min^{-1}) for 1 h. Then He was introduced and the temperature was cooled down to at 25 °C. The CO (9.6% CO in He) pulses were intermittently injected into the carrier gas, and the CO gas was detected using a TCD.

The TOL selectivity S_{TOL} assuming a pseudo-first order kinetics shown in Fig. 1c and d can be described with conversion X as follows:

$$S_{TOL} = \left\{ \frac{k_1}{k_2 - k_1 - k_3} \left((1-X) - (1-X)^{\frac{k_2}{k_1+k_3}} \right) \right\} / X$$

The measured metal content is listed in Table S1.

Table S1 Metal content of mono- and bi-metallic catalysts measured by ICP analyses.

Catalyst	Metal content (wt%)		M/Ni ratio
	Ni	M	-
Pt	0	1	-
Ni	6.7	0	-
Ag	0	0.5	-
Sn	0	6.76	-
Zn	0	8.7	-
In	0	8.17	-
Ni-Ag	4.88	0.74	0.15
Ni-Sn	5.08	1.36	0.27
Ni-Zn	5.81	3.54	0.55
Ni-In	5.63	1.26	0.22

Fig. S1 Scanning transmission electron microscope (STEM) images of the reduced Ni/Al_2O_3, and $NiZn_{0.6}/Al_2O_3$.

Ni **$NiZn_{0.6}$**

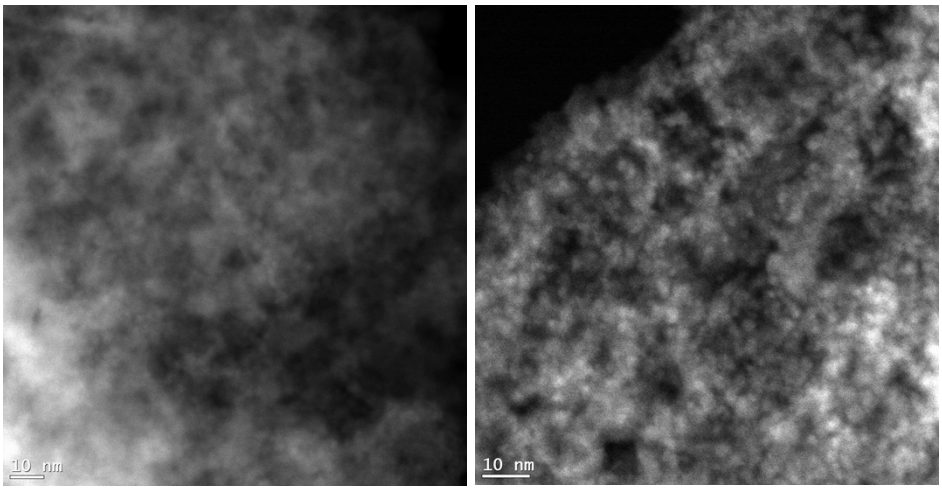

The XRD patterns of the reduced mono-metallic (Ni and Zn) and bi-metallic (Ni-$Zn_{0.1}$ and Ni-$Zn_{0.6}$) catalysts supported on Al_2O_3 are shown in Fig. S2. For the Ni/Al_2O_3 catalyst, peaks are expected at a 2θ of 44.4, 51.8 and 76.3 for metallic Ni, which was difficult to identify because of high background originating from Al_2O_3. For the Zn/Al_2O_3 catalyst, the small peaks shown in the XRD patterns suggested the presence of hexagonal ZnO. It was challenging to clearly distinguish between Ni and Zn supported Al_2O_3 due to the very small crystallite size (approximately 2 to 5 nm) confirmed by HRTEM (Fig. 2 in the main manuscript).

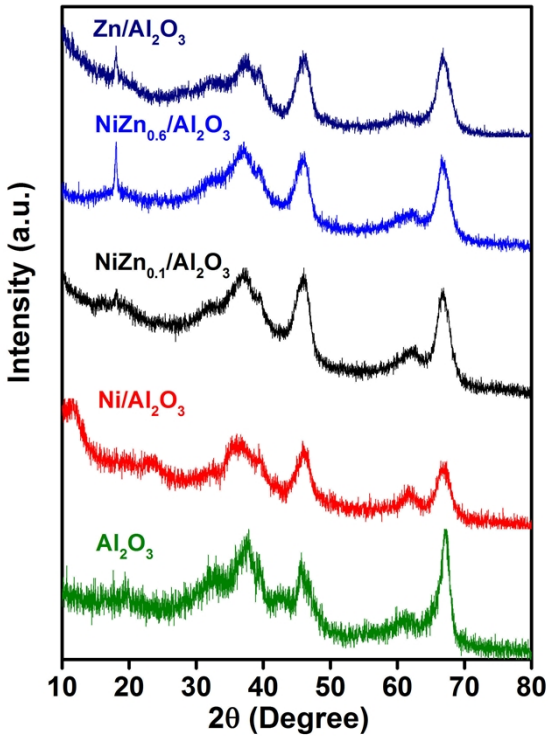

Fig. S2 Powder XRD patterns of the reduced mono- and bi-metallic Ni-based catalysts: a) γAl_2O_3, b) Ni/Al_2O_3, c) $NiZn_{0.1}/Al_2O_3$, d) $NiZn_{0.6}/Al_2O_3$ and e) Zn/Al_2O_3.

Computational details

We performed electronic structure calculations based on density functional theory (DFT) using the revised Perdew-Burke-Ernzerhof (revPBE) exchange-correlation functional as implemented in the VASP [1-4] code. Plane-wave basis sets (with a kinetic energy cutoff of 350 eV [5]) were used to describe the valence electrons (i.e., 10 electrons of Ni ($3d^8 4s^2$) and 12 electrons of Zn ($3d^{10} 4s^2$)). We employed a 0.1 eV smearing of the Fermi-level, (8×8×8) K-points for bulk calculations and (4×4×1) K-points for surfaces. The core electrons were replaced by projector augmented wave (PAW) pseudopotentials.[6,7] The relaxation of the atomic positions in the supercell occurred until the energy differences were smaller than 0.01 eV/Å. With this setup, we simulated the electronic structure of the Ni/Zn alloys, the substitution of one Ni by a Zn atom in Ni nanoparticles, and the substitution of a Ni atom by a Zn atom on regular Ni surfaces with (100), (111) and (211) facets.

For the geometric study, we considered a cluster and a surface model. The cluster model was represented by icosahedral and cuboctrahedral Ni_{55} nanoparticles. Because VASP is a periodic code, these clusters were placed in a repeating cubic box with an edge that was sufficiently large to prevent interactions between the images (more than 10 Å between the successive images). The surface model corresponds to a Ni surfaces with (100), (111) and (211) facets. The facets were modeled with slabs that consisted of four atomic layers. We used a p(3×3) supercell with a 12 Å vacuum that was perpendicular to the surface. The modification of the surface was performed by replacing a Ni atom from the top layer with a Zn atom.

Ni_{55} nanoparticles with 1 Zn atom:

To understand the preference of Zn to be embedded in the bulk or at the surface of a regular Ni structure, we performed cluster model calculations using a 55 Ni atom cluster with icosahedron and cuboctahedron symmetries (Fig. S3). The icosahedron structure (Ih) was more stable than the cuboctahedron structure (Oh) by 3.75 eV, and this structure was used in the following calculations. Next, we modeled a series of $Ni_{54}Zn$ clusters where the Zn atom replaced a Ni atom in the icosahedron Ni_{55} cluster at different positions. On the surface, which corresponds to the second Ni shell, the Zn atom can be placed on a corner or an edge. The geometries with the Zn atom at these

positions are the most stable (0.01 eV difference). Using these structures as the reference structure at 0 eV, the geometry with the Zn atom in the first coordination shell was 1.63 eV higher in energy, and the geometry with the Zn atom at the center of the cluster was 1.51 eV higher in energy. Overall, these results indicate that the Zn atom prefers to be on the surface rather than in the core of the NPs, and this result was confirmed using different cluster sizes consisting of 13, 55 and 147 atoms.

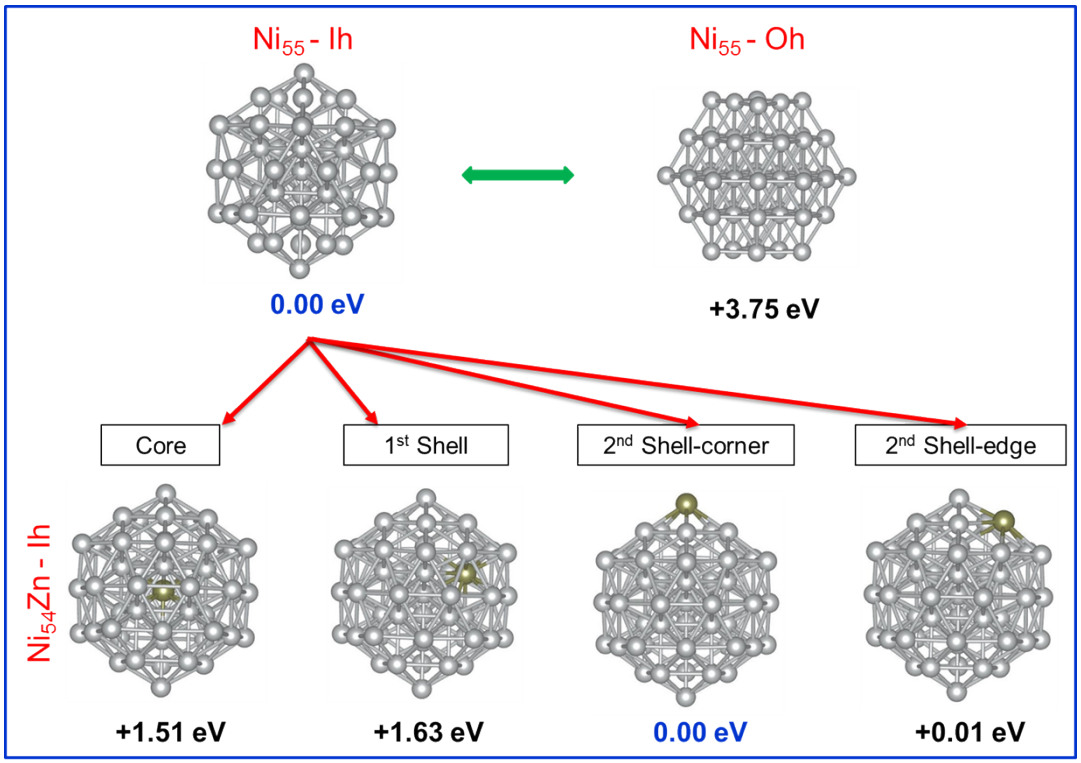

Fig. S3 Energetic comparison between Ni_{55}-Icosahedron and Ni_{55}-Cuboctahedron and energy difference when a Ni atom is replaced by a Zn atom in different positions of the icosahedron.

Ni (hkl) surfaces with a Zn atom:

To determine the stabilities of the possible geometrical configurations occurring at the surface of Ni/Zn alloys, we modeled the effect of replacing one Ni atom by a Zn atom. Specifically, we considered the (100), (111) and (211) Ni facets (Fig. S4). The first two facets are flat but have different atom densities with the highest density on the (111) facet and different binding sites (i.e., 4-fold and 3-fold sites on the (100) and (111) facets, respectively). The (211) facet is stepped with

3 different types of Ni atoms that range from highly saturated at the bottom of the step to highly unsaturated at the ridge of the step. Although we have clear evidence that with the high Zn concentrations on the surface, the real alloys will result in surfaces that cannot be represented by a model consisting of a single Zn atom on a pure Ni surface, these models can offer insights in to local situations (i.e., if the Zn prefers to sit on flat surfaces, leaving the step sites to the Ni, or vice versa).

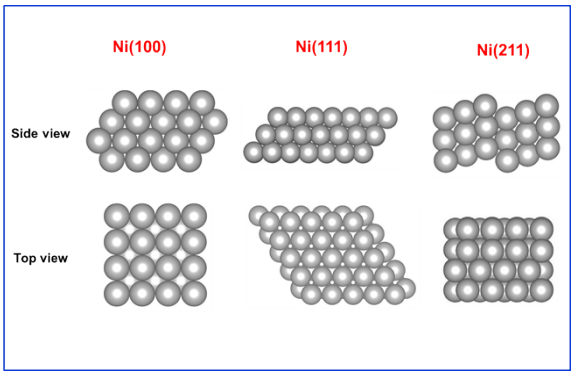

Fig. S4 Side and top views of the (100), (111) and (211) facets of the fcc nickel crystal.

In this section, one Ni atom on the surface as replaced by one Zn atom. The optimization of the structures leads to a slight geometrical deformation with a small displacement in the Zn atom out of the (100) and (111) surfaces. This result is reasonable based on the difference between the atomic radii of Ni and Zn (i.e., 124 pm for Ni compared to 134 pm for Zn). From an energetic perspective, the energy of substitution (E_{Sub}) was calculated as expressed in Eq. S1:

$$Ni_n(hkl) + Zn = Ni_{n-1}Zn(hkl) + Ni \qquad \text{Eq. S1}$$

The E_{Sub} values calculated for the different facets are reported in Table S2. Using the lowest E_{Sub}, which corresponds to the replacement of a Zn atom on the ridge of the (211) facet and the geometry indicated as Position 1 in Fig. S5, the relative stability of the different facets with a Zn atom can be calculated using Eq. S2, and these values are reported in Figure S4.

$$\Delta E_{Sub}(hkl) = E_{Sub}(hkl) - E_{Sub}(211)/1 \qquad \text{Eq. S2}$$

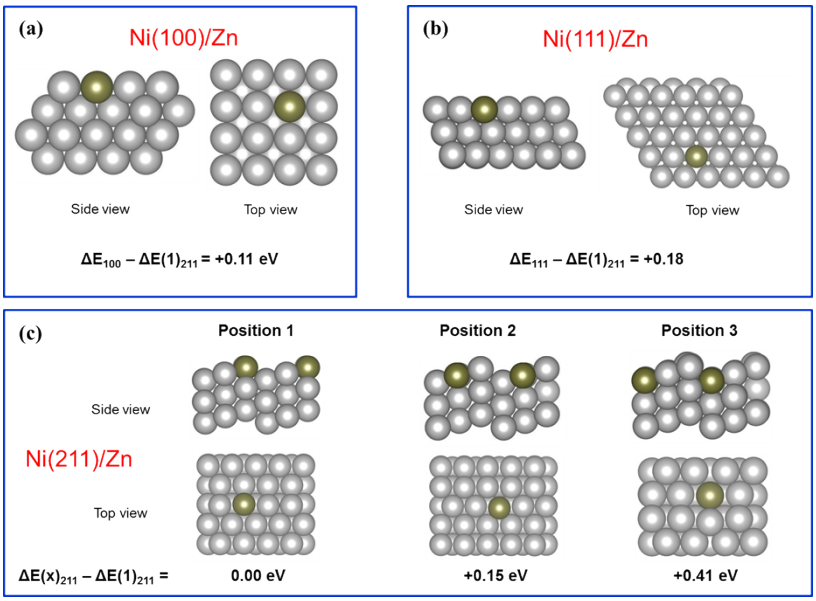

Fig. S5 Side and top views of the (100), (111) and (211) facets of fcc nickel crystal where one Ni atom is replaced by a Zn atom. Only one atom has been replaced, and the second atom shown in the side view is due to the periodicity of the slabs.

Table S2 Preferred Zn site tested by replacing one Ni atom with a Zn atom on the three surfaces (i.e., (100), (111) and (211)). The number of atoms and cell parameters for each surface are listed. *E* is the total energy of the system, and E_{Sub} is the energy difference between that of the system with one Ni atom replaced by a Zn atom and that of the pure Ni system.

Surface	N. atoms (Ni/Zn)	a (Å)	b (Å)	c (Å)	ϒ (°)	*E* (eV)	E_{Sub}(eV)
Ni(100)	36/0	7.341	7.341	15.128	90	−177.41	-
Ni(100)/Zn	35/1					−174.11	3.30
Ni(111)	48/0	9.853	9.853	15.930	120	−236.55	-
Ni(111)/Zn	47/1					−233.19	3.36
Ni(211)	27/0	7.343	6.030	21.734	90	−131.99	-
Ni(211)/Zn1	26/1					-128.80	**3.19**
Ni(211)/Zn2	26/1					-128.64	3.35
Ni(211)/Zn3	26/1					-128.38	3.61

References

(1) Kresse, G.; Furthmüller, J. *Phys. Rev. B* **1996**, *54*, 11169.

(2) Kresse, G.; Hafner, J. *Phys. Rev. B* **1993**, *47*, 558.

(3) Kresse, G.; Hafner, J. *Phys. Rev. B* **1994**, *49*, 14251.

(4) Kresse, G.; Hafner, J. *J. Mater. Sci.* **1996**, *6*, 15.

(5) Studt, F.; Abild-Pedersen, F.; Bligaard, T.; Sørensen, R. Z.; Christensen, C. H.; Nørskov, J. K. *Angewandte Chemie International Edition* **2008**, *47*, 9299.

(6) Blöchl, P. E. *Phys. Rev. B* **1994**, *50*, 17953.

(7) Kresse, G.; Joubert, D. *Phys. Rev. B* **1999**, *59*, 1758.